Title

Rise in Northeast US extreme precipitation caused by Atlantic variability and climate change

Authors

Huang, Huanping

Patricola, Christina M

Winter, Jonathan M

et al.

Publication Date

2021-09-01

DOI

10.1016/j.wace.2021.100351

Peer reviewed

Weather and Climate Extremes 33 (2021) 100351

Contents lists available at ScienceDirect

Weather and Climate Extremes

journal homepage: www.elsevier.com/locate/wace

Rise in Northeast US extreme precipitation caused by Atlantic variability and climate change

Huanping Huang [a,*], Christina M. Patricola [b,a], Jonathan M. Winter [c,d], Erich C. Osterberg [d], Justin S. Mankin [c,d,e]

[a] Climate and Ecosystem Sciences Division, Lawrence Berkeley National Laboratory, Berkeley, CA, USA
[b] Department of Geological and Atmospheric Sciences, Iowa State University, Ames, IA, USA
[c] Department of Geography, Dartmouth College, Hanover, NH, USA
[d] Department of Earth Sciences, Dartmouth College, Hanover, NH, USA
[e] Lamont-Doherty Earth Observatory of Columbia University, Palisades, NY, USA

ARTICLE INFO

Keywords:
Extreme precipitation
Atlantic sea surface temperatures
Anthropogenic forcings
Atlantic multidecadal variability
Optimal fingerprinting
Time of detection

ABSTRACT

Extreme precipitation (EP) in the Northeastern United States increased abruptly after 1996, coinciding with warming Atlantic sea surface temperatures (SSTs). We examine the importance of internal variability and external forcings (including anthropogenic and natural forcings) to these EP and SST increases by using the Community Earth System Model large ensembles and an optimal fingerprint method to isolate the effects of different forcings on 1929–2018 Northeast EP and North Atlantic SSTs. We find that external forcings have significantly influenced both Northeast EP and North Atlantic SSTs, with a time of detection in 2008 and 1968, respectively. Beyond SST changes attributable to internal variability of the Atlantic, anthropogenic aerosols and greenhouse gases are important drivers of SST changes, first detected in 1968 and 1983, respectively. Greenhouse gases are the only anthropogenic forcing exerting substantial influence on EP, first detected in 2008. We therefore attribute the 1996 EP shift to both unforced Atlantic variability and anthropogenic forcings.

1. Introduction

Extreme precipitation (EP), defined as precipitation falling on the 1% of wet days recording the most precipitation, has increased rapidly in the Northeastern United States (hereafter Northeast; Fig. 1) over the past century (Frei et al., 2015; Hayhoe et al., 2018; Hoerling et al., 2016; Huang et al., 2017b; Kunkel et al., 2013). Among U.S. climate regions, the Northeast had the fastest increase (55%) in EP since 1958 and the second fastest increase (38%) since 1901 (Hayhoe et al., 2018). This EP increase occurred abruptly in 1996, with average 1996–2014 EP being 53% higher than average 1901–1995 EP, leading to higher flood risks (Collins, 2019; Dupigny-Giroux et al., 2018; Frei et al., 2015; Huang et al., 2017b; Peterson et al., 2013). For instance, in the state of Vermont, EP from Tropical Storm Irene in 2011 caused the state's worst disaster since 1927, costing $733 million (Minter, 2012). As such, understanding the causes of the EP increase since 1996 is crucial to correctly interpreting future simulations of EP, and ultimately the range of EP impacts the Northeast needs to be prepared for.

The observed change in Northeast EP is qualitatively consistent with the expected change in EP based on the Clausius–Clapeyron relation, i.e., about a 7% increase in saturation vapor pressure for every °C of warming (Easterling et al., 2017; Ivancic and Shaw, 2016; Kunkel et al., 2013), as well as more frequent weather systems causing EP events (Huang et al., 2018; Kunkel et al, 2010, 2012, 2013; Marquardt Collow et al., 2016). In particular, 48% of the abrupt 1996 EP increase was caused by tropical cyclones likely due to warmer Atlantic sea surface temperatures (SSTs) and higher total column water vapor, with frontal systems (25%) and extratropical cyclones (15%) also contributing (Huang et al., 2018).

Because of their importance in shaping tropical cyclones—and thus EP increases across the Northeast—Atlantic SSTs warrant further investigation. Variations in Atlantic SSTs are linked to low-frequency variability at multidecadal time scales, anthropogenic climate change, natural forcings, and inter-basin teleconnections with the El Niño-Southern Oscillation (Enfield and Mayer, 1997; Gillett et al., 2008; Goldenberg et al., 2001; Mann et al., 2021). There is considerable work that points to the low-frequency variability being influenced by anthropogenic forcings (Bellomo et al., 2018; Murphy et al., 2017; Si

* Corresponding author.
E-mail address: huanpinghuang@lbl.gov (H. Huang).

https://doi.org/10.1016/j.wace.2021.100351
Received 20 January 2021; Received in revised form 24 June 2021; Accepted 2 July 2021
Available online 3 July 2021

et al., 2017), external volcanic and solar forcings (Mann et al., 2021; Otterå et al., 2010), and internal ocean variability (Kim et al., 2018b; Zhang et al., 2019). We therefore refer to multidecadal variability in the Atlantic as simply Atlantic multidecadal variability (AMV). The AMV shift from a cold to warm phase around 1995 appears to play a significant role in boosting Northeast EP through enhanced tropical cyclone activity (Curtis, 2008; Huang et al., 2018; Kunkel et al., 2010). Thus, investigating the cause of the North Atlantic SST warming and the AMV shift is an essential step towards understanding the causes of the Northeast EP rise in 1996.

Global change in EP has been attributed to anthropogenic forcing (Bindoff, 2013; Dittus et al., 2016; Fischer and Knutti, 2015; Min et al., 2011; Zhang et al., 2013), but confidence in attributing EP changes at regional scales has been limited and less robust (Easterling et al., 2017; Sarojini et al., 2016). The barriers to robust detection and attribution include observational uncertainty, climate model uncertainty, and internal variability (Dittus et al., 2016; Easterling et al., 2017; Martel et al., 2018; Sarojini et al., 2016). For example, a formal attribution of the role of anthropogenic forcing on Northeast EP change from 1979 to 2013 was not conclusive due to internal decadal ocean variability and climate models' inability to capture the multi-decadal trend in observed EP (Hoerling et al., 2016). Kirchmeier-Young and Zhang (2020) found that external forcings did contribute to the increase in 1961–2010 precipitation extremes over North America (including the Northeast). However, the relative importance of internal variability and different anthropogenic forcings on the 1996 Northeast EP shift, as well as the associated SST changes, remains unresolved.

To address the challenge of attributing Northeast EP change, we leveraged the Community Earth System Model version 1 (CESM1) large ensemble simulations and an optimal fingerprint method to disentangle the roles of internal variability and individual anthropogenic forcings on the observed changes in North Atlantic SSTs and Northeast EP. The optimal fingerprint method (Hasselmann, 1993) assumes that observed climate change can be estimated as a linear combination of model-derived spatial or temporal patterns of external forcing (i.e., "the fingerprint") plus a residual term that is attributable to the real world trajectory of internal variability (see Section 2.3 for details). The noise of internal climate variability usually hinders the detection and attribution of anthropogenic effects in any single realization or small ensemble (Deser et al., 2020a; Santer et al., 2019). We avoided this limitation by using the recently available CESM1 large ensemble single forcing simulations (Deser et al., 2020b) to isolate selected anthropogenic influences on regional climate from the noise of internal variability.

2. Data and methods

2.1. Observational and climate model data

Observational precipitation data are from the Global Historical Climatology Network-Daily (GHCN-D), the official archive for U.S. daily weather observations (Menne et al., 2012). To reduce the influence of missing observational records on estimating regional precipitation change, we selected a subset of high-quality weather stations by requiring them to have at least 80% of complete daily records from 1920 to 2018 (Winter et al., 2020). Two hundred and twenty stations met this criterion in the Northeastern US spanning from Maine to West Virginia (Fig. 1). Any years in these stations with less than 80% of daily observations are treated as missing and eliminated from the analysis (Winter et al., 2020). Observations-based sea surface temperatures over the North Atlantic basin are retrieved from the newest version (v5) of the Extended Reconstructed Sea Surface Temperature (ERSST) dataset (Huang et al., 2017a). This dataset provides global monthly sea surface temperature at a 2° × 2° spatial resolution from January 1854 to present.

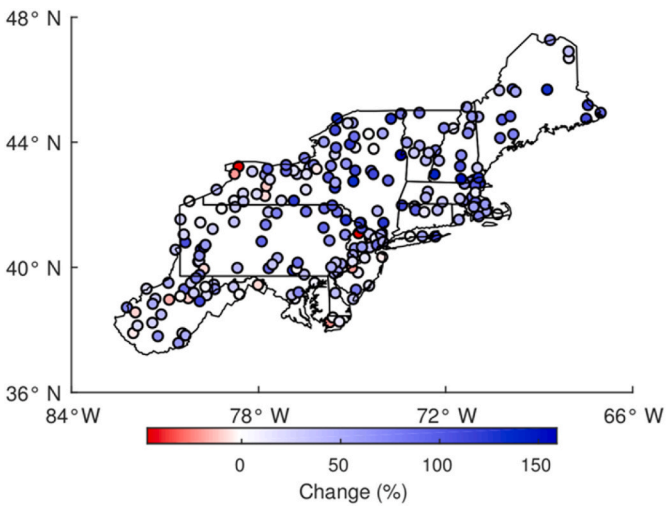

Fig. 1. Relative change in annual extreme precipitation across GHCN-D stations. The change denotes the percentage difference during 1996–2018 as compared to 1920–1995. The subset of 220 GHCN-D weather stations in the Northeastern US has at least 80% of complete daily records from 1920 to 2018 at each station.

To attribute the changes in North Atlantic SSTs and Northeast EP to different external forcings, we used the outputs from two sets of fully-coupled CESM1 experiments performed at a 1° horizontal resolution. The first set is from the CESM1 Large Ensemble (LENS) Project, which is an initial condition large ensemble (40 members) simulating transient climate from 1920 to 2100 (Kay et al., 2015). Each ensemble member is run with the same time-evolving radiative forcing (including anthropogenic and natural forcings), with historical forcings from 1920 to 2005 and RCP8.5 forcings thereafter. But each member is run with slightly different initial conditions (air temperature field randomly perturbed at the level of round-off error; Kay et al., 2015). Thus each member is consistent with the same forcing, and the distribution of climates across all realizations is a robust estimate of CESM1's representation of internal climate variability (Deser et al., 2020b; Kay et al., 2015; Mankin et al., 2020). We merged the historical simulations (1920–2005) with a portion of RCP8.5 simulations (2006–2018) to form 40 transient simulations covering the period from 1920 to 2018 with the presence of all known historical forcings (ALL). The second set of climate simulations comes from the CESM1 Single Forcing Ensemble Project (Deser et al., 2020b). Its model configurations, initial conditions, and radiative forcings are the same as the LENS project, except that one of the four anthropogenic forcing agents is fixed at its 1920 level while the other forcings follow historical and projected changes (Deser et al., 2020b). The experimental design creates four smaller initial condition ensembles within the Single Forcing Ensemble Project, each of which simulates a counterfactual climate without one of four anthropogenic forcing agents. This "leave-one-out" experimental design is applied to four forcing agents: greenhouse gases (XGHG, 20 members), industrial aerosols (XAER, 20 members), biomass burning aerosols (XBMB, 15 members), and land use and land change (XLULC, 5 members). As with the ALL ensemble, we combined the historical (1920–2005) with a portion of the projection (2006–2018) to create a set of 1920–2018 transient simulations with each single forcing ensemble. As it takes several years for the ocean response to diverge from the same initial conditions across all ensemble members, we discarded the first nine years of simulations and keep the remaining 90 years (1929–2018) for the analysis.

Each realization from each ensemble can be considered a combination of signal (i.e., the forced response, estimated as the time-evolving mean across each ensemble) and noise (internal variability, estimated

as the residual of each ensemble member with the ensemble mean removed). Thus, the contribution of a single forcing agent to a climate response (e.g., a change in SSTs or EP) is estimated by subtracting the time-evolving ensemble mean of a single forcing ensemble from the ensemble mean of historical simulations with all forcings (ALL_{em}) (Deser et al., 2020b), as shown in equations (1)–(4) for each of the forcing agents.

$$GHG_{em,t} = ALL_{em,t} - XGHG_{em,t} \quad (1)$$

$$AER_{em,t} = ALL_{em,t} - XAER_{em,t} \quad (2)$$

$$BMB_{em,t} = ALL_{em,t} - XBMB_{em,t} \quad (3)$$

$$LULC_{em,t} = ALL_{em,t} - XLULC_{em,t} \quad (4)$$

Here *em* refers to ensemble mean of each ensemble (i.e., the forced response; Mankin et al., 2020), and t is the year, ranging from 1929 to 2018. Because each realization is signal plus noise, the combined effect of a single forcing and internal variability from ensemble member i is calculated by adding each ensemble member's climate variability to the single forcing response (Deser et al., 2020b), as illustrated in equations (5)–(8).

$$GHG_{i,t} = (XGHG_{i,t} - XGHG_{em,t}) + GHG_{em,t} \quad (5)$$

$$AER_{i,t} = (XAER_{i,t} - XAER_{em,t}) + AER_{em,t} \quad (6)$$

$$BMB_{i,t} = (XBMB_{i,t} - XBMB_{em,t}) + BMB_{em,t} \quad (7)$$

$$LULC_{i,t} = (XLULC_{i,t} - XLULC_{em,t}) + LULC_{em,t} \quad (8)$$

2.2. Analysis methods

We analyzed the temporal and spatial changes in SSTs over the North Atlantic basin (0–60° N, 0–80° W), as well as EP in the Northeast. Here EP is defined as the amount of precipitation falling on the 1% of wet days recording the most precipitation (Huang et al., 2017b, 2018). We determine the EP threshold based on all daily records spanning from 1929 to 2018 by weather station (for GHCN-D) or grid cell (for CESM1). Then we calculate annual accumulated EP exceeding the threshold. Lastly, we perform 1°×1° gridded area averaging (spatial resolution of CESM1 simulations) to calculate regional average EP for GHCN-D observations and CESM1 outputs. SSTs and EP are computed separately for the CESM1 historical (ALL) and single forcing (XGHG, XAER, XBMB, and XLULC) simulations. To evaluate the long-term trend in SSTs, we used simple linear regression (parametric method) with a Student's t-test. For Northeast EP, we used the Theil–Sen robust linear regression (nonparametric method) with the modified Mann–Kendall test for autocorrelated data (Hamed and Rao, 1998).

To quantify the relative roles of internal variability and external forcings on Atlantic multidecadal variability (AMV), we estimated the AMV as the well-defined Atlantic Multidecadal Oscillation index using the ERSST observations and CESM1 simulations. The index is defined as the multidecadal variability of SST anomalies over the North Atlantic (0–60° N, 0–80° W), which has a period of approximately 70 years (Kerr, 2000). We calculated AMV by averaging North Atlantic SSTs over the domain and then detrending the time series of SST anomalies (Enfield et al., 2001). Numerous studies evaluate different methods to quantify AMV, and how well CESM1 and other climate models simulate Atlantic variability, including the observed magnitude and the timing of its phase shifts (Bellomo et al., 2018; Frankignoul et al., 2017; Mann et al., 2017; Si et al., 2017). By linearly detrending the North Atlantic SST anomalies, Bellomo et al. (2018) and Si et al. (2017) found that the CESM1-LENS generally reproduces the observed AMO (defined here as identical to AMV) in both the preindustrial and the ensemble mean of the ALL simulations as well as the timing of phase shifts in the ALL ensemble, but not the observed AMO magnitude. Other studies have found model-derived AMO is the artifact of computation methods (especially linear detrending) which leave behind residual forced effects, and further suggested that AMO is absent in most climate model simulations (Frankignoul et al., 2017; Mann et al., 2020). Given that the CESM1-LENS ensemble has been extensively evaluated against the AMV (Bellomo et al., 2018; Frankignoul et al., 2017; Si et al., 2017), the current study focuses on using the CESM1 ALL and single forcing simulations to assess the effects of external forcings and internal variability on observed SST anomalies, and how the anomalies are compared with AMV in observations. We applied different detrending methods to quantify AMV, facilitating a comparison with past studies.

To account for the nonlinearity of individual forced responses, we detrended SST anomalies by subtracting a quadratic trend (Enfield and Cid-Serrano, 2010) or the ALL ensemble mean trend (Mann et al., 2020) from observations. We also used linear detrending (Enfield et al., 2001) to compute AMV that is comparable with other CESM1 LENS-based studies (Bellomo et al., 2018; Si et al., 2017), despite the fact that it may leave behind residual forced effects (Frankignoul et al., 2017; Mann et al., 2014). To evaluate how each individual forcing affects observed SST anomalies and estimated AMV, we subtracted the ensemble mean trends in the four single forcing simulations from the observations as in Qin et al. (2020). So the residual SSTs from detrending a single forcing's effect contain internal variability and changes by forcing agents (Qin et al., 2020). Further, we combined the four single forcings as Bellomo et al. (2018) to represent the overall effect of anthropogenic forcings on SSTs.

2.3. Fingerprint method

The optimal fingerprint method (Hasselmann, 1993) is widely used to detect and attribute climate change (Bindoff, 2013; Hegerl and Zwiers, 2011; Stone et al., 2009), including sea surface temperatures (Gillett et al., 2008) and extreme precipitation (Easterling et al., 2016; Min et al., 2011; Zhang et al., 2013). This method treats observed changes in a climate variable, Y, as a linear combination of model-derived spatial or temporal patterns of external forcing F (i.e., "fingerprint") with residual internal variability, ε, as described in equation (9):

$$Y_{obs} = \sum_{i=1}^{m} (F_i - \varepsilon_i)\beta_i + \varepsilon \quad (9)$$

Here Y_{obs} represents an observational climate variable, such as SST and EP. F_i refers to the ith forcing of m external forcings (signals) considered, such as all anthropogenic and natural forcings combined (ALL), greenhouse gases (GHG), industrial aerosols (AER), biomass burning (BMB), land use and land cover (LULC), and all-but-one forcing (XGHG, XAER, XBMB, and XLULC). ε_i is sampling noise arising from using a small ensemble to estimate the forced response pattern (Allen and Stott, 2003). β_i is the regression coefficient (i.e., scaling factor) regarding amplitude errors in the model-derived forced signal F_i. ε is the noise term linked to internal climate variability in the observations. The noise terms, ε_i and ε, are assumed to share the same covariance structure (Allen and Stott, 2003).

Here we conducted one-signal (ALL forcings) and two-signal (GHG vs. XGHG, AER vs. XAER, BMB vs. XBMB, and LULC vs. XLULC forcings) detection and attribution analyses by using the regularized optimal fingerprinting (ROF) method (Ribes et al., 2013). This ROF method is based on a regularized estimate of the covariance structure of climate variability, avoiding a truncation of the empirical orthogonal functions implemented in the standard optimal fingerprinting method (Allen and Stott, 2003). Thus it provides a more objective and accurate implementation of optimal fingerprinting (Ribes et al., 2013). We solved the regression model (equation (9)) with the total least square approach, which is included in the ROF function provided through the Environment Canada's Optimal Fingerprint package (Feng, 2014), deriving the best estimate of scaling factors and their confidence intervals (CIs).

We first calculated regionally averaged SST and EP anomalies 1929–2018 (baseline period 1929–1958) in both observations and ensemble averaged forced responses (such as $GHG_{em,t}$ in equation (1)) and then converted them into non-overlapping 5-year means. We used 5-year means to reduce the temporal dimension of climate data, making the covariance matrix a more reasonable size, while maintaining the short term features of climate variables (Kirchmeier-Young and Zhang, 2020; Wan et al., 2015). Next, we used the CESM1-LENS preindustrial control simulations (Kay et al., 2015) to estimate internal climate variability and then computed two independent covariance matrices C_1 and C_2. Specifically, the control simulations were divided into 90-year time series by creating a 90-year sliding window and moving it 10 years at a time (1–90, 11–100, 21–110, and so on). This yielded 170 time series of climate noise data representing internal climate variability, with each time series represented by 18 non-overlapping 5-year anomalies (relative to their respective first 30-year period). The 170 chunks were divided into two parts (i.e., 85 time series each) to construct C_1 and C_2, respectively. C_1 was used for prewhitening observations and forced responses (i.e. optimization) and then estimating scaling factors, and C_2 was applied to conduct an uncertainty analysis on the resulting scaling factors (Allen and Stott, 2003; Ribes et al., 2013). If the 90% CI of the resulting scaling factors β is above 0, then the fingerprint from an individual forcing is detected in the observations and significant at the 0.05 level. When the signal is detected, the CI containing 1 indicates the model-derived forced response is consistent with the observations. The CI above (below) 1 suggests the forced response has to be scaled up (down) to be comparable with the observations, which is to account for climate model's limitation in simulating the magnitude of forced response (Hegerl and Zwiers, 2011; Mitchell and Karoly, 2001). CI of β below 0 indicates that the forced response contributes to an opposite trend of observed climate change, possibly due to climate model error in simulating the forced response. Lastly, we conducted a residual consistency check (Ribes et al., 2013) to evaluate the agreement between the regression residual in equation (9) and the assumed internal variability from the CESM1-LENS preindustrial control simulations. If the evaluation is passed, the regression model is considered suitable and raises confidence in the detection results. If the test is rejected, the regression model should be revised to account for incorrect simulated forced responses or low internal variability (Ribes et al., 2013).

Besides attributing climate change during the full time period 1929–2018, we also implemented a sensitivity test for scaling factors based upon moving time periods. Specifically, we held the start date in each period fixed in 1929 while its end date was moved from 1963 to 2018 with an interval of five years. This is to ensure that we have long enough records (>30 years) to conduct detection and attribution and maximize the signal to noise ratio (Mitchell and Karoly, 2001). The date when a forced signal emerged from internal variability and became detectable is called the time of detection (Carter et al., 2019).

3. Results and discussion

3.1. Observed and simulated changes in North Atlantic sea surface temperatures

We find that CESM1 reasonably simulates the spatial and temporal patterns of North Atlantic (0–60° N, 0–80° W) SST changes from 1929 to 2018 (Fig. 2a and b and 3a), consistent with earlier studies (Chemke et al., 2020; Kim et al., 2018a; Si et al., 2017). The variability of observed SSTs lies within the CESM1 historical all-forcings (ALL, which include anthropogenic and natural forcings) ensemble range ($p = 0.11$, Kolmogorov-Smirnov, hereafter K–S test). From 1929 to 2018, the observed and ALL ensemble-mean SSTs increased by 0.55 and 0.45 °C century^{-1} ($p < 0.001$), respectively, despite temporarily cooling around 1970 (Fig. 3a). All 40 ensemble members reproduce the significant warming trends through the 1929–2018 period (95% CI: 0.29–0.61 °C century^{-1}). This demonstrates that the CESM1 model is capable of simulating regional SSTs, facilitating the detection and attribution of SST changes and their relationship with the Northeast EP increases.

3.2. Anthropogenic influences on North Atlantic sea surface temperatures

We subtract the single forcing simulations from ALL to determine the influence of each forcing, and find contrasting effects of different radiative forcings on SSTs (Fig. 2c–f and 3b). Starting from 1929, anthropogenic greenhouse gases (GHG) warmed the North Atlantic basin by 0.8 °C century^{-1} ($p < 0.01$; 95% CI from ensemble members: 0.65–0.96 °C century^{-1}; Figs. 2c and 3b). Conversely, industrial aerosols (AER) cooled SSTs significantly at a rate of −0.17 °C century^{-1} ($p < 0.01$; 95% CI: −0.30 to −0.03 °C century^{-1}; Figs. 2d and 3b). Our GHG and AER findings are consistent with earlier studies (Dunstone et al., 2013; Ting et al., 2015). Biomass burning (BMB) and land use and land cover (LULC) have minor to negligible influences on SSTs (Fig. 2e–f and 3b), approximately equivalent to one tenth of the effects from GHG and AER. While the warming effect from GHG increased monotonically over 1929–2018, the cooling effect of industrial AER intensified until the 1970s and then slowly dampened afterwards (Fig. 3b), a result of

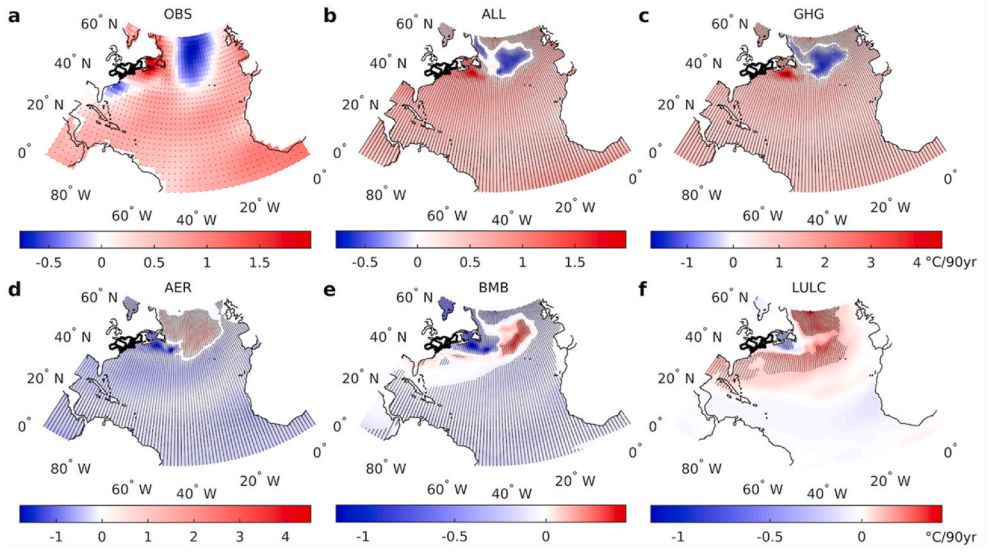

Fig. 2. Spatial patterns of 1929–2018 trends in North Atlantic sea surface temperatures (SSTs, °C per 90 yr) in the ERSST v5 observations (OBS, a), CESM1 historical all-forcings simulations (ALL, b), and single-forcing simulations for greenhouse gases (GHG, c), aerosols (AER, d), biomass burning (BMB, e), and land use and land cover (LULC, f). b-f are from the ensemble mean. Stippling indicates a significant change in the SST time series at the 0.05 level using the Student's t-test. Note that the scales in a-b are different from c-d and e-f. The land region covering the Northeastern US, the study area for extreme precipitation change, is highlighted by thick black lines.

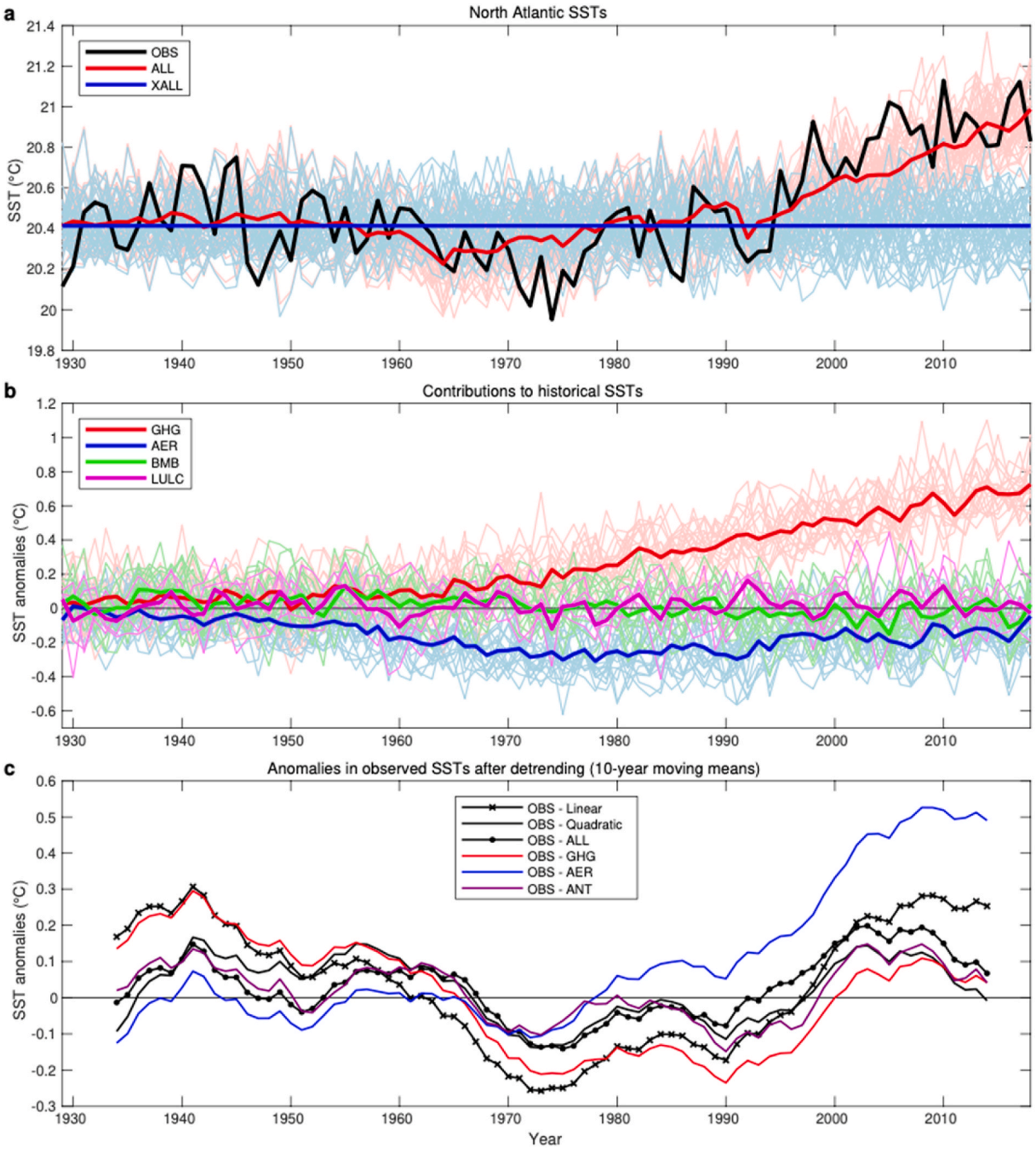

Fig. 3. Temporal changes in sea surface temperatures (SSTs) over the North Atlantic (0–60° N, 0–80° W). a, Time series of 1929–2018 SSTs in the ERSST v5 observations (OBS), CESM1 historical all-forcings simulations (ALL), and detrended ALL simulations by removing the time-evolving ALL ensemble mean (XALL). b, Contributions of greenhouse gases (GHG, red lines), aerosols (AER, blue lines), biomass burning (BMB, green lines), and land use and land cover (LULC, magenta lines) to historical ALL SSTs. Thick lines in a and b represent the ensemble mean, while thin lines are individual ensemble members and indicate ensemble spreads. c, Anomalies in observed SSTs after detrending by removing linear trend (Linear), quadratic trend (Quadratic), and trends estimated from ALL, GHG, AER, and the four anthropogenic single forcings combined (ANT) ensemble means, respectively. A 10-year smoothing window is applied and the anomalies are calculated relative to a baseline period 1929–1998. (For interpretation of the references to colour in this figure legend, the reader is referred to the Web version of this article.)

environmental legislation passed in North America and Europe around 1970 that substantially decreased aerosol emissions (Deser et al., 2020b; Myhre et al., 2013).

Spatially, the opposing effects of GHG (warming) and AER (cooling) are evident over the entire North Atlantic basin (Fig. 2). However, the basin average effects imposed by GHG and AER are reversed in the subpolar North Atlantic (i.e., warming by AER and cooling by GHG) (Fig. 2c and d). This area overlaps with the well-documented North Atlantic warming hole in observations and climate models (Drijfhout et al., 2012). The physical mechanisms of the North Atlantic warming hole are not explored in this study, but previous research has linked the warming hole to a weakening of the Atlantic Meridional Overturning Circulation (AMOC) (Caesar et al., 2018; Chemke et al., 2020; Cheng et al., 2013; Drijfhout et al., 2012; Gervais et al., 2018). While a weakening AMOC may be associated with natural variability (Chen and Tung, 2018; Zhang, 2008), it has also been associated with rising CO_2 concentrations in both observations and climate models (Caesar et al., 2018; Chemke et al., 2020; Saba et al., 2016). The warming over the

Arctic has increased sea ice melt and river runoff, leading to higher freshwater fluxes through the Arctic gates (between Greenland and the Canadian Arctic Archipelago), freshened surface water, reduced Labrador Sea deep convection, and ultimately a cooling of the Labrador Sea (Gervais et al., 2018). This is supported by the spatial pattern of cooling in Fig. 2c. In contrast, the faster warming near the Northeast has been connected to the northward shift of the Gulf Stream as a result of the AMOC slowdown (Caesar et al., 2018). The opposite seesaw patterns in Fig. 2c and d reflect competing thermodynamic effects by GHG and AER on SSTs. Even though the overall effect by BMB is close to neutral, it actually exerted a cooling influence over a large part of the North Atlantic (Fig. 2e), a result of increased BMB aerosols in the South America and Canada and decreased BMB aerosols in the US since 1929 (Deser et al., 2020b; Granier et al., 2011). As expected, the influence by LULC is marginal across space (Fig. 2f).

The anthropogenic and natural forcings of ALL, especially anthropogenic GHG and AER, play significant roles in driving the observed SST changes, especially over the past four decades (Fig. 4). Regression of the ALL fingerprint (one-signal) onto the observed 1929–2018 SST anomalies show that the signal is detectable at the 0.05 significance level (Fig. 4b). The 90% CI of scaling factors for the ALL fingerprint (1.07–1.52) is above 0, with the best estimate at 1.29. Simultaneous regression of the GHG and XGHG fingerprints (two-signal) onto the observed SSTs shows that both fingerprints are detectable. The 90% CIs of scaling factors for GHG (1.1–1.57) and XGHG (1.04–1.91) are above 0, with the best estimates at 1.33 and 1.46, respectively. Similarly, the fingerprints of AER and XAER are detected, with their 90% CIs of scaling factors at 1.19–2.17 and 1.03–1.52. These demonstrate that GHG and AER are largely responsible for historical SST changes over the North Atlantic. Two-signal analysis with the BMB and XBMB fingerprints yields similar results as using the LULC and XLULC fingerprints. Despite detectable BMB and LULC fingerprints, plugging their best-estimate scaling factors (3.58 for BMB and 4.36 for LULC) into the regression equation (9) reveals that each fingerprint minimally contributed to the

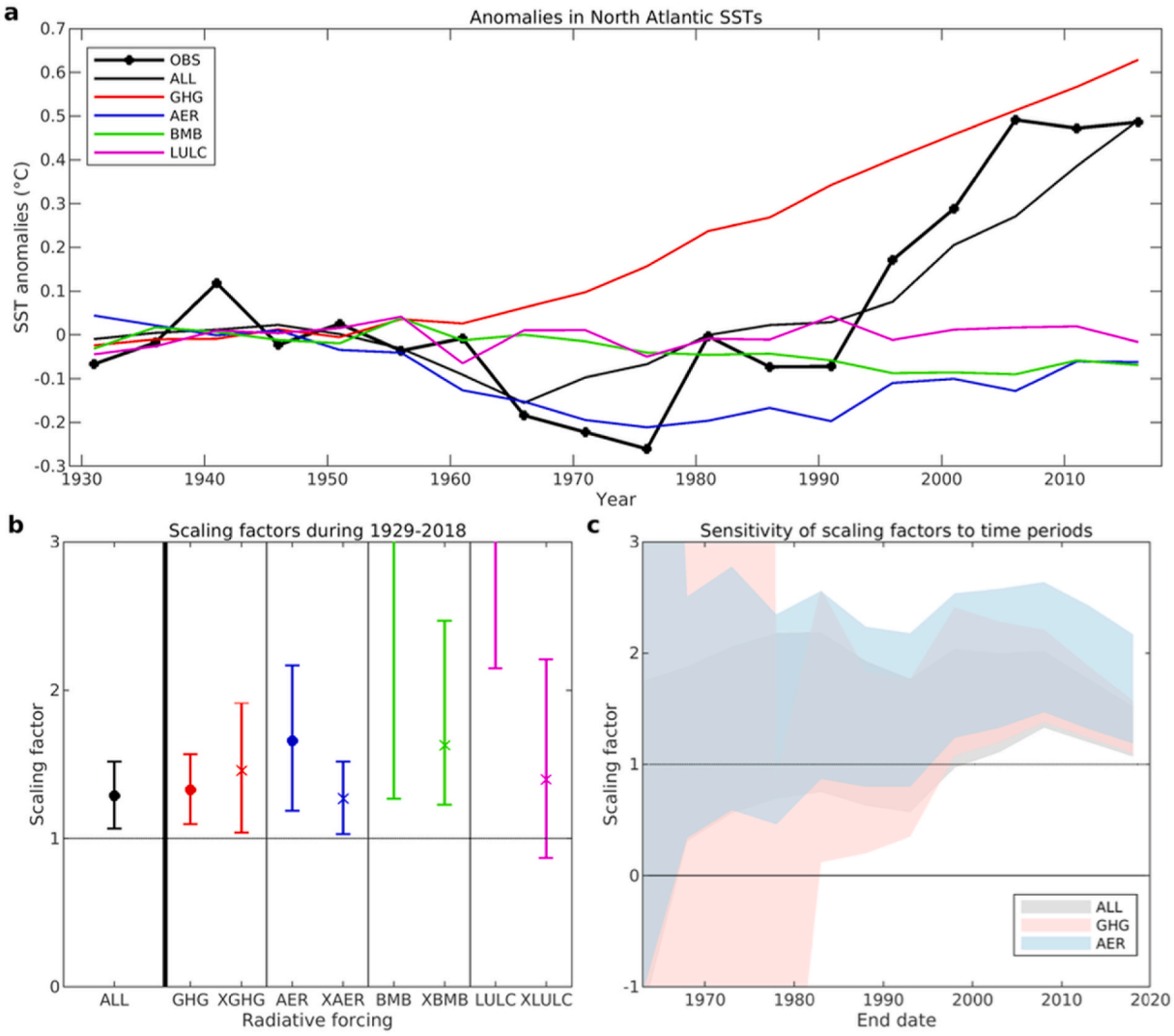

Fig. 4. Optimal fingerprint detection of North Atlantic sea surface temperatures (SSTs) change. a, SST anomalies over the North Atlantic in the ERSST v5 observations (OBS), ensemble-averaged CESM1 historical all-forcings simulations (ALL, including anthropogenic and natural), and the four ensemble-averaged CESM1 single forcing simulations (GHG: greenhouse gases, AER: aerosols, BMB: biomass burning, and LULC: land use and land cover), all represented by non-overlapping 5-year means and relative to 1929–1958. b, Scaling factors for North Atlantic SSTs from one-signal (ALL forcings) and two-signal (GHG vs. XGHG, AER vs. XAER, BMB vs. XBMB, and LULC vs. XLULC forcings) regressions over the time period 1929–2018. c, Scaling factors for ALL, GHG, and AER over varying time periods with an interval of 5 years (i.e., with a fixed start date in 1929 but a moving end date as designated on the x-axis). Circles and crosses in b indicate the best estimates of scaling factors, and error bars in b and shaded areas in c represent the 90% confidence intervals for scaling factors. Confidence intervals extending beyond the figure represent large uncertainties of scaling factors. A signal is detectable when the confidence interval is above zero, and the forced response is consistent with observations when the confidence interval contains one.

observed SST changes. In contrast, XBMB and XLULC fingerprints (both including GHG and AER forcings) are primarily responsible for historical SST changes. Furthermore, residual consistency checks are passed for these one- and two-signal analyses, adding confidence to the detection results while underlying the importance of both GHG and AER effects in leading to historical SST changes. We further tested when the important fingerprints become detectable by alternating the time period considered in the one- and two-signal analyses. Specifically, the start date is held constant in 1929 and the end date spans 1963 to 2018 at an interval of five years. Fig. 4c shows that the ALL and AER fingerprints were first detected in 1968, while the GHG fingerprint emerged in 1983. The XAER (including GHG and other forcings) and XGHG (including AER and other forcings) fingerprints were also first detected in 1983 (not shown), confirming the timing when GHG and AER forcings started to accelerate the observed SST warming.

Is the AMV (defined here identical to AMO, detrended SST anomalies

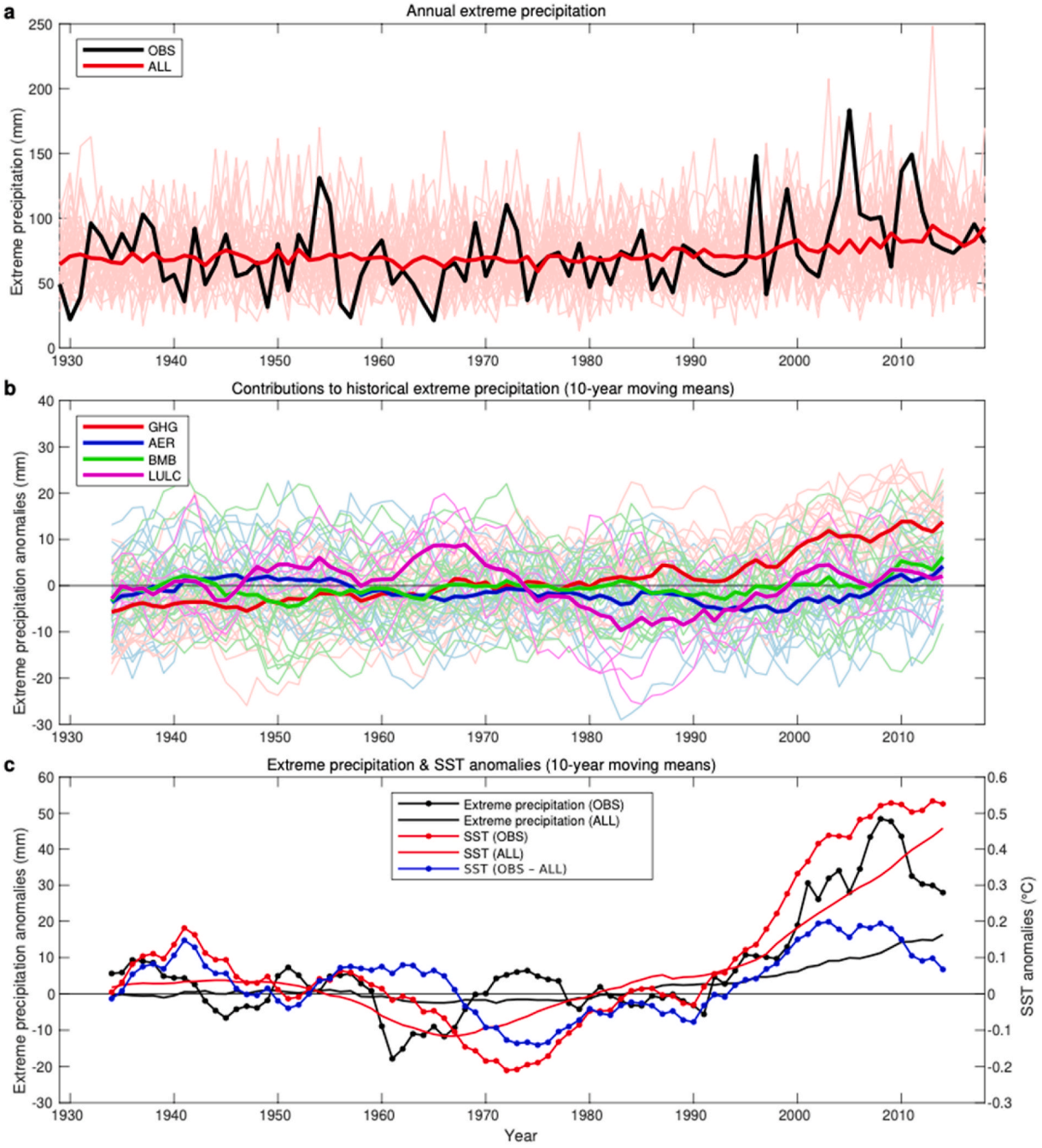

Fig. 5. Temporal changes in extreme precipitation over the Northeastern US. a, Time series of 1929–2018 annual extreme precipitation in the GHCN-D observations (OBS) and CESM1 historical all-forcings simulations (ALL, including anthropogenic and natural). b, Extreme precipitation anomalies attributed to greenhouse gases (GHG, red lines), aerosols (AER, blue lines), biomass burning (BMB, green lines), and land use and land cover (LULC, magenta lines), as compared to ALL extreme precipitation. Thick lines in a and b represent ensemble mean, while thin lines are individual ensemble members and indicate model spreads. c, Anomalies in Northeast extreme precipitation and North Atlantic sea surface temperatures (SSTs). The anomalies in observed SST after removing the ALL ensemble-averaged trend (OBS - ALL) are an indicator of the Atlantic Multidecadal Variability. Anomalies in extreme precipitation and SSTs are relative to the baseline period 1929–1998. Lines in b and c are smoothed with a 10-year moving mean. (For interpretation of the references to colour in this figure legend, the reader is referred to the Web version of this article.)

averaged over 0–60° N, 0–80° W) a natural mode or driven by natural and anthropogenic forcings? Previous studies have found anthropogenic forcings are major drivers of AMV changes, especially in the late twentieth century (Bellomo et al., 2018; Si et al., 2017), while others argue that the AMV is primarily a natural mode in the climate system (Kim et al., 2018b; Zhang et al., 2019), or a combination of both (Enfield and Cid-Serrano, 2010; Ting et al., 2014). By using simulations from the Coupled Model Intercomparison Project Phase 5, Mann et al. (2021, 2020) argued the AMV during the preindustrial era (1000–1835 CE) is exclusively caused by volcanic radiative forcing, and the AMV during the historical era (1850–2005) is driven by natural and anthropogenic forcings, rather than internal multidecadal oscillations. Here we examined this question by calculating the AMV in observations with different trends removed, and used the CESM1 ALL and single forcing simulations to assess the effects of external forcings and internal variability on SST anomalies (see Section 2.2 for details). Fig. 3c shows that the AMV estimated by removing the time-evolving ALL ensemble mean produces the same three phases (warm–cold–warm) as the linearly detrended AMV, with relatively small differences (less than a decade) in the timing of phase shifts. The former method leads to significantly smaller magnitudes of AMV ($p < 0.01$, K–S test) during all phases when compared to that from linear detrending, consistent with earlier findings (Bellomo et al., 2018; Mann et al., 2014; Si et al., 2017). In contrast, the AMV from removing the quadratic trend highly resembles the ALL-detrended AMV ($p = 0.74$), highlighting the ability of the quadratic trend to remove most external forcings. The evidence suggests that the observation-based AMV may have an internal variability component. Nevertheless, almost none of the individual ALL ensemble members (detrended with the ALL ensemble mean) can reproduce the AMV (Fig. 3a), implying some limitation with the CESM1 model in simulating the observed AMV correctly. Interestingly, only the SST anomalies created by removing the SST trend induced by AER significantly differ from the ALL-detrended SST anomalies. The SST anomalies created by removing the SST trends induced by GHG or anthropogenic forcings combined (including GHG, AER, BMB, and LULC) are not significantly different from the ALL-detrended SST anomalies (Fig. 3c). The evidence further suggests that the observed AMV is significantly modulated by AER. In summary, Figs. 2–4 confirm that GHG (AER) exerted a warming (cooling) effect on the observed SST changes. SST warming since the 1980s was mostly caused by strengthened warming from GHG and reduced cooling from AER, with some contribution from internal variability as well.

3.3. Observed and simulated changes in Northeast extreme precipitation

The ALL simulations perform well in simulating annual EP and its change over the Northeast (Fig. 5a). The observed EP in GHCN-D experienced an abrupt increase in 1996, characterized by a 48% increase in annual EP during 1996–2018 as compared to 1929–1995 (Fig. 5a), consistent with an earlier study (Huang et al., 2017b). In the ALL simulations, a similar EP changepoint is detected in the late 1990s (1998), even though the magnitude of ensemble-averaged EP increase (17% when comparing 1996–2018 to 1929–1995) is smaller than the observed change. The observed (GHCN-D) and simulated (ALL) EP increased by 3.2 and 1.4 mm decade^{-1} ($p < 0.01$), respectively, from 1929 to 2018, but had no significant trends from 1929 to 1995 prior to the changepoint. The variability of observed EP lies within the ALL ensemble range ($p = 0.9997$, K–S test), and most of the ALL ensemble members (37 out of 40) have the same sign of upward trends from 1929 to 2018 (95% CI: –0.2 to 3.2 mm decade^{-1}). This evidence suggests the CESM1 model is able to reproduce the change (including the 1996 shift) in observed EP, making the attribution of the EP abrupt shift feasible.

3.4. Anthropogenic impacts on Northeast extreme precipitation

Anthropogenic GHG are a crucial driver of the recent increase in EP, while other forcings are not (Fig. 5b). The increase in observed EP can only be reproduced with the presence of anthropogenic GHG, and none of the other anthropogenic forcings are important in capturing the change in EP, especially the post-1996 shift. A decomposition of individual forcings shows that the overall effect of GHG led to an increase of 2.3 mm decade^{-1} ($p < 0.01$) of EP from 1929 to 2018, and all 20 ensemble members have the same sign of upward trends (95% CI: 1.0–3.7 mm decade^{-1}). The ensemble average of BMB effect increased EP slightly by 0.5 mm decade^{-1} ($p < 0.05$) from 1929 to 2018, and the increase is only evident during the most recent decade. Its 95% CI of EP trends for ensemble members (−1.4 to 2.6 mm decade^{-1}) includes 0, indicating some uncertainty in the impact of BMB on Northeast EP due to internal climate variability. Aerosols produced from BMB in the US have steadily decreased over the past century (Deser et al., 2020b; Granier et al., 2011), and therefore BMB's impact on EP over the last decade is potentially anomalous. In fact, when we include the last decade (2019–2029) in the XBMB ensemble, we discover that the impact of BMB on Northeast EP drops to essentially zero (not shown). This implies the BMB-related EP increase during the most recent decade could be a result of model variability, similar to the decadal variations of LULC-related EP. The contributions from AER and LULC to EP are not statistically significant, and their 95% CIs of EP change center around 0, as demonstrated by their ensemble means and individual members (Fig. 5b). We note that EP variations associated with LULC may be due to its small ensemble size (5) and the LULC effect on post-1996 EP change remains insignificant.

Fig. 6 further demonstrates that ALL forcings are responsible for the observed change in EP, with anthropogenic GHG as a critical driving force. The fingerprint of ALL forcings is detected at the 0.05 significance level, with the CI of scaling factors ranging from 1.41 to 3.43 (Fig. 6b). Based on our two-signal analyses over 1929–2018, all fingerprints are detectable except XBMB. Specifically, the 90% CI of scaling factors for GHG (XGHG) is 1.76–42.19 (1.00–118.87) with a best estimate of 3.56 (5.55). We note that the large scaling factors indicate the model-derived GHG and XGHG effects on EP have to be substantially scaled up to be comparable with the observed EP. Despite detectable fingerprints by other forcings, incorporating their best-estimate scaling factors into the regression equation (9) reveals that no fingerprint other than GHG has a major impact on the observed EP changes. BMB appears to influence EP, but its effect is much less important than XBMB. Residual consistency checks are generally passed for these one- and two-signal analyses, adding confidence to the detection results. We also tested the sensitivity of our detection results over various time lengths by moving the end date from 1963 to 2018 with an interval of five years (start date fixed in 1929). This analysis further confirms that GHG are the primary forcing detectable in the observations (Fig. 6c). The forced signal by GHG reached a detectable level in 2008, with the same timing as the ALL forced signal. Unlike SSTs, the effect of AER on Northeast EP is muted, confirming the mixed impacts of increased aerosols on Northeast EP (Ntelekos et al., 2009). According to Ntelekos et al. (2009), this can be explained by the highly nonlinear interactions between the AER-related thermodynamic and microphysical processes involved in intense convective storms, and the sensitivity of each storm to regional meteorological conditions.

Our results are consistent with Kirchmeier-Young and Zhang (2020) who found the fingerprint of external forcing on 1961–2010 EP change in a broader Northeast region by using the same ROF method and three large ensembles of climate model data (including CESM1). Martel et al. (2018) found the time of detection in 2030 over the eastern North America region, which is two decades later than our findings. This may be due to the averaging with other subregions (e.g., southeastern US) which has experienced a much smaller increase in EP than over the Northeast (Easterling et al., 2017) and therefore delayed the time of detection.

Fig. 5c shows a strong correlation between EP and SSTs from 1929 to 2018, with a higher correlation in the ALL simulations (0.85) than in observations (0.48). Furthermore, the correlation between the ALL-

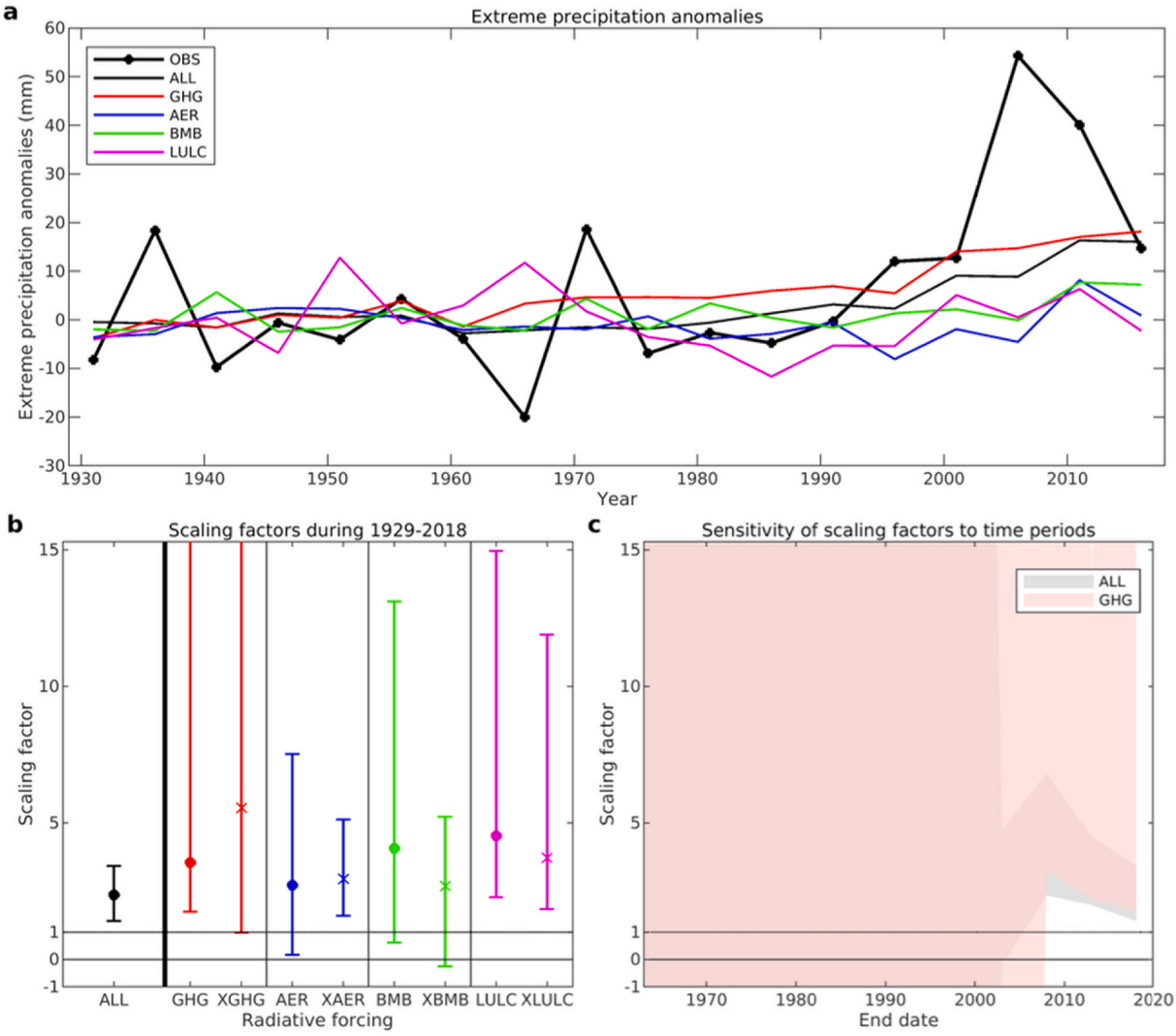

Fig. 6. Optimal fingerprint detection of Northeast extreme precipitation change. a, Extreme precipitation anomalies over the Northeastern US in the GHCN-D observations (OBS), ensemble-averaged CESM1 historical all-forcings simulations (ALL), and the four ensemble-averaged CESM1 single forcing simulations (GHG: greenhouse gases, AER: aerosols, BMB: biomass burning, and LULC: land use and land cover), all represented by non-overlapping 5-year means and relative to 1929–1958. b, Scaling factors for Northeast extreme precipitation from one-signal (ALL forcings) and two-signal (GHG vs. XGHG, AER vs. XAER, BMB vs. XBMB, and LULC vs. XLULC forcings) regressions over the time period 1929–2018. c, Scaling factors for ALL and GHG over varying time periods with an interval of 5 years (i.e., with a fixed start date in 1929 but a moving end date as designated on the x-axis). Circles and crosses in b indicate the best estimates of scaling factors, and error bars in b and shaded areas in c represent the 90% confidence intervals for scaling factors. Confidence intervals extending beyond the figure represent large uncertainties of scaling factors. A signal is detectable when the confidence interval is above zero, and the forced response is consistent with observations when the confidence interval contains one.

simulated EP and SSTs is stronger from 1996 to 2018 (0.75, $p < 0.01$) than from 1929 to 1995 (0.39, $p < 0.01$), consistent with the relationship between observed EP and SSTs. Taken together, the evidence indicates that the CESM1 model closely reproduces the relationship between EP and SSTs, and a linear relationship between EP and SST was enhanced after 1996. Similarly, the GHG-forced EP and SST responses from 1929 to 2018 are strongly correlated (0.66, $p < 0.01$), especially after 1996. Combined with our finding of a strong GHG influence on SSTs (especially since 1983), these results support our hypothesis that GHG influenced Northeast EP via increased SSTs.

Recent studies have tied the reduced aerosol loadings in the Atlantic basin since 1970 to an increased number of Atlantic tropical storms (Dunstone et al., 2013; Murakami et al., 2020) and higher potential intensity (Sobel et al., 2016; Ting et al., 2015), thus contributing to more frequent major hurricanes (Murakami et al., 2018). Starting from the late 1990s, the warming of SSTs from increased GHG and reduced AER is approximately twice the warming from the cold-to-warm AMV shift (Fig. 3c), both of which facilitate the development of more major hurricanes (Villarini and Vecchi, 2013). However, relative to anthropogenic forcings, there is evidence (Camargo et al., 2013; Ting et al., 2015) that AMV was the more likely cause of the sharp increase in hurricane potential intensity, especially since 1995. We also find that both observed and ALL-simulated EP are significantly correlated with the AMV during the current AMV warm phase since 1996 ($p \leq 0.05$), as shown in Fig. 5c. It is worth noting that EP did decrease during the last AMV cold phase (1963–1995) after the shift from the previous AMV warm phase (1928–1962), though they are not significantly different (Huang et al., 2018). In this study, we explicitly connect the anomalously high EP since 1996 to both the AMV shift and anthropogenic-driven SST warming, likely through inducing more tropical storms that have made a large contribution (48%) to the Northeast EP shift (Huang et al., 2018; Murakami et al., 2020).

Our application of the CESM1 large ensembles to conduct detection and attribution provides a robust estimation of forced responses and

detection results (Deser et al., 2020b; Santer et al., 2019), especially when compared to those using a smaller number of climate realizations. However, there are some caveats to our approach. We caution that detecting and attributing EP change at local scales and other regions remains highly uncertain due to the challenges outlined in the introduction, importantly the large noise of internal variability (Martel et al., 2018). Further, the CESM1 climate simulations are too coarse in horizontal resolution (1-degree latitude/longitude) to explicitly resolve many physical processes (e.g., moist-adiabatic temperature lapse rate and vertical velocity) and thus the accurate representations of tropical cyclones and extreme precipitation (Ntelekos et al., 2009; Roberts et al., 2020; van der Wiel et al., 2016). As seen in Fig. 5a, both the EP upward trend over 1929 to 2018 and shift after 1996 are much higher in observed EP than in simulated EP. These barriers hamper a more robust detection and attribution. To improve future attribution studies, it will be important to leverage state-of-the-art GCMs, especially those run over higher resolutions and cloud-resolving scales, such as the CMIP6 High Resolution Model Intercomparison Project (Haarsma et al., 2016).

4. Conclusions

We find that historical ALL forcings (including anthropogenic and natural) have exerted significant influences on North Atlantic SSTs and Northeast EP over the period from 1929 to 2018, with their time of detection in 1968 and 2008, respectively. Increased anthropogenic GHG and reduced AER warmed the North Atlantic, and BMB and LUCL have minor to negligible influences on SSTs. The times of detection for the AER and GHG fingerprints on SSTs are 1968 and 1983, respectively. We also find that observed AMV is significantly driven by AER and may have an internal ocean variability component that is not well captured by the CESM1 model.

For Northeast EP, GHG are the only anthropogenic forcing of significance, with the GHG fingerprint detectable since 2008. Our detection and attribution results are based upon the CESM1 model's reasonable performance in simulating the spatial and temporal patterns of North Atlantic SSTs and Northeast EP. The model can also closely reproduce the correlation between observed EP and SSTs, which strengthened after 1996. Recent SST warming, a result of increased GHG and reduced AER, is a key factor responsible for the post-1996 increase in Northeast EP, though the effect from AMV is also important. Therefore, according to our analysis of the CESM1 runs, the 1996 shift in Northeast EP can be attributed to both climate variability (especially AMV) and anthropogenic forcings (especially GHG), rather than either factor alone. Given the projected increase in GHG emissions, we expect that extreme precipitation across the Northeastern US will continue to rise, though potentially muted over the next few decades by a shift to AMV negative conditions.

Data availability

The Global Historical Climatology Network-Daily (GHCN-D) precipitation data are available from the National Centers for Environmental Information (NCEI) under National Oceanic and Atmospheric Administration (https://data.nodc.noaa.gov/cgi-bin/iso?id=gov.noaa.ncdc:C00861#). The Extended Reconstructed Sea Surface Temperature (ERSST) v5 data are also obtained from NCEI (https://www.ncdc.noaa.gov/data-access/marineocean-data/extended-reconstructed-sea-surface-temperature-ersst-v5). Climate model data are outputs from the CESM1 Large Ensemble Community Project and CESM1 Single Forcing Large Ensemble Project, both led by the National Center for Atmospheric Research (NCAR), with supercomputing resources provided by NSF/CISL/Yellowstone and the University of Toronto, and archived at the NCAR Climate Data Gateway (www.earthsystemgrid.org).

CRediT authorship contribution statement

Huanping Huang: Conceptualization, Methodology, Software, Formal analysis, Writing – original draft, Visualization, Validation. **Christina M. Patricola:** Conceptualization, Methodology, Resources, Writing – review & editing, Supervision. **Jonathan M. Winter:** Conceptualization, Methodology, Resources, Writing – review & editing, Supervision. **Erich C. Osterberg:** Conceptualization, Methodology, Resources, Writing – review & editing, Supervision. **Justin S. Mankin:** Conceptualization, Methodology, Resources, Writing – review & editing, Supervision.

Declaration of competing interest

The authors declare that they have no known competing financial interests or personal relationships that could have appeared to influence the work reported in this paper.

Acknowledgements

This material was supported by the U.S. Department of Energy, Office of Science, Office of Biological and Environmental Research, Climate and Environmental Sciences Division, Regional & Global Model Analysis Program, under Award Number DE-AC02-05CH11231, and the Vermont Established Program for Stimulating Competitive Research (NSF Award OIA 1556770). Analyses were performed on the Discovery Cluster and HPC environments supported by the Research Computing group, IT&C at Dartmouth College. We acknowledge the CESM Project and supercomputing resources provided by NSF/CISL/Yellowstone for offering access to the CESM1 large ensembles. We thank Yang Feng of Environment and Climate Change Canada for creating and providing the ECOF (Environment Canada's Optimal Fingerprint) package, in which the regularized optimal fingerprint (ROF) function was translated from the ROF package V0.8 by Aurélien Ribes. We also thank Dáithí Stone and Xuebin Zhang for their insight regarding the application of optimal fingerprinting.

References

Allen, M.R., Stott, P.A., 2003. Estimating signal amplitudes in optimal fingerprinting, part I: Theory. Clim. Dynam. https://doi.org/10.1007/s00382-003-0313-9.

Bellomo, K., Murphy, L.N., Cane, M.A., Clement, A.C., Polvani, L.M., 2018. Historical forcings as main drivers of the Atlantic multidecadal variability in the CESM large ensemble. Clim. Dynam. https://doi.org/10.1007/s00382-017-3834-3.

Bindoff, 2013. Detection and attribution of climate change: from global to regional. Climate Change 2013 the Physical Science Basis: Working Group I Contribution to the Fifth Assessment Report of the Intergovernmental Panel on Climate Change. https://doi.org/10.1017/CBO9781107415324.022.

Caesar, L., Rahmstorf, S., Robinson, A., Feulner, G., Saba, V., 2018. Observed fingerprint of a weakening Atlantic Ocean overturning circulation. Nature. https://doi.org/10.1038/s41586-018-0006-5.

Camargo, S.J., Ting, M., Kushnir, Y., 2013. Influence of local and remote SST on North Atlantic tropical cyclone potential intensity. Clim. Dynam. https://doi.org/10.1007/s00382-012-1536-4.

Carter, B.R., Williams, N.L., Evans, W., Fassbender, A.J., Barbero, L., Hauri, C., Feely, R. A., Sutton, A.J., 2019. Time of detection as a metric for prioritizing between climate observation quality, frequency, and duration. Geophys. Res. Lett. https://doi.org/10.1029/2018GL080773.

Chemke, R., Zanna, L., Polvani, L.M., 2020. Identifying a human signal in the North Atlantic warming hole. Nat. Commun. https://doi.org/10.1038/s41467-020-15285-x.

Chen, X., Tung, K.-K., 2018. Global surface warming enhanced by weak Atlantic overturning circulation. Nature 559, 387–391. https://doi.org/10.1038/s41586-018-0320-y.

Cheng, W., Chiang, J.C.H., Zhang, D., 2013. Atlantic meridional overturning circulation (AMOC) in CMIP5 Models: RCP and historical simulations. J. Clim. https://doi.org/10.1175/JCLI-D-12-00496.1.

Collins, M.J., 2019. River flood seasonality in the Northeast United States: characterization and trends. Hydrol. Process. https://doi.org/10.1002/hyp.13355.

Curtis, S., 2008. The Atlantic multidecadal oscillation and extreme daily precipitation over the US and Mexico during the hurricane season. Clim. Dynam. 30, 343–351. https://doi.org/10.1007/s00382-007-0295-0.

Deser, C., Lehner, F., Rodgers, K.B., Ault, T., Delworth, T.L., DiNezio, P.N., Fiore, A., Frankignoul, C., Fyfe, J.C., Horton, D.E., Kay, J.E., Knutti, R., Lovenduski, N.S.,

Marotzke, J., McKinnon, K.A., Minobe, S., Randerson, J., Screen, J.A., Simpson, I.R., Ting, M., 2020a. Insights from Earth system model initial-condition large ensembles and future prospects. Nat. Clim. Change. https://doi.org/10.1038/s41558-020-0731-2.

Deser, C., Phillips, A.S., Simpson, I.R., Rosenbloom, N., Coleman, D., Lehner, F., Pendergrass, A.G., Stevenson, S., 2020b. Isolating the evolving contributions of anthropogenic aerosols and greenhouse gases: a new CESM1 large ensemble community resource. J. Clim. https://doi.org/10.1175/JCLI-D-20.

Dittus, A.J., Karoly, D.J., Lewis, S.C., Alexander, L.V., Donat, M.G., 2016. A multiregion model evaluation and attribution study of historical changes in the area affected by temperature and precipitation extremes. J. Clim. https://doi.org/10.1175/JCLI-D-16-0164.1.

Drijfhout, S., van Oldenborgh, G.J., Cimatoribus, A., 2012. Is a decline of AMOC causing the warming hole above the North Atlantic in observed and modeled warming patterns? J. Clim. https://doi.org/10.1175/JCLI-D-12-00490.1.

Dunstone, N.J., Smith, D.M., Booth, B.B.B., Hermanson, L., Eade, R., 2013. Anthropogenic aerosol forcing of Atlantic tropical storms. Nat. Geosci. https://doi.org/10.1038/ngeo1854.

Dupigny-Giroux, L.A., Mecray, E.L., Lemcke-Stampone, M.D., Hodgkins, G.A., Lentz, E. E., Mills, K.E., Lane, E.D., Miller, R., Hollinger, D.Y., Solecki, W.D., Wellenius, G.A., Sheffield, P.E., MacDonald, A.B., Caldwell, C., 2018. Northeast. In: Impacts, Risks, and Adaptation in the United States: Fourth National Climate Assessment, ume II. https://doi.org/10.7930/NCA4.2018.CH26.

Easterling, D.R., Kunkel, K.E., Arnold, J.R., Knutson, T.R., LeGrande, A.N., Leung, L.R., Vose, R.S., Waliser, D.E., Wehner, M., 2017. Precipitation change in the United States. In: Climate Science Special Report: Fourth National Climate Assessment. Forth Natioanl Clim. Assessment, I I. https://doi.org/10.7930/J0H993CC.U.S, 207–230.

Easterling, D.R., Kunkel, K.E., Wehner, M.F., Sun, L., 2016. Detection and attribution of climate extremes in the observed record. Weather Clim. Extrem. https://doi.org/10.1016/j.wace.2016.01.001.

Enfield, D.B., Cid-Serrano, L., 2010. Secular and multidecadal warmings in the North Atlantic and their relationships with major hurricane activity. Int. J. Climatol. https://doi.org/10.1002/joc.1881.

Enfield, D.B., Mayer, D.A., 1997. Tropical atlantic sea surface temperature variability and its relation to El Niño-Southern Oscillation. J. Geophys. Res. C Oceans. https://doi.org/10.1029/96jc03296.

Enfield, D.B., Mestas-Nunez, A.M., Trimble, P.J., 2001. The Atlantic Multidecadal Oscillation and its relationship to rainfall and river flows in the continental. U.S. Geophys. Res. Lett. 25, 2077–2080. https://doi.org/10.1029/2000GL012745.

Feng, Y., 2014. Tutorials on environment Canada's optimal fingerprint package [WWW Document]. URL. https://www.wcrp-climate.org/ictp-2014-tutorials.

Fischer, E.M., Knutti, R., 2015. Anthropogenic contribution to global occurrence of heavy-precipitation and high-temperature extremes. Nat. Clim. Change. https://doi.org/10.1038/nclimate2617.

Frankignoul, C., Gastineau, G., Kwon, Y.O., 2017. Estimation of the SST response to anthropogenic and external forcing and its impact on the Atlantic multidecadal oscillation and the Pacific decadal oscillation. J. Clim. https://doi.org/10.1175/JCLI-D-17-0009.1.

Frei, A., Kunkel, K.E., Matonse, A., 2015. The seasonal nature of extreme hydrological events in the northeastern United States. J. Hydrometeorol. 16, 2065–2085. https://doi.org/10.1175/JHM-D-14-0237.1.

Gervais, M., Shaman, J., Kushnir, Y., 2018. Mechanisms governing the development of the North Atlantic Warming Hole in the CESM-LE future climate simulations. J. Clim. https://doi.org/10.1175/JCLI-D-17-0635.1.

Gillett, N.P., Stott, P.A., Santer, B.D., 2008. Attribution of cyclogenesis region sea surface temperature change to anthropogenic influence. Geophys. Res. Lett. https://doi.org/10.1029/2008GL033670.

Goldenberg, S.B., Landsea, C.W., Mestas-Nunez, A.M., Gray, W.M., 2001. The recent increase in Atlantic hurricane activity: causes and implications. Science 293, 474–479. https://doi.org/10.1126/science.1060040.

Granier, C., Bessagnet, B., Bond, T., D'Angiola, A., van der Gon, H.D., Frost, G.J., Heil, A., Kaiser, J.W., Kinne, S., Klimont, Z., Kloster, S., Lamarque, J.F., Liousse, C., Masui, T., Meleux, F., Mieville, A., Ohara, T., Raut, J.C., Riahi, K., Schultz, M.G., Smith, S.J., Thompson, A., van Aardenne, J., van der Werf, G.R., van Vuuren, D.P., 2011. Evolution of anthropogenic and biomass burning emissions of air pollutants at global and regional scales during the 1980-2010 period. Climatic Change 109, 163–190. https://doi.org/10.1007/s10584-011-0154-1.

Haarsma, R.J., Roberts, M.J., Vidale, P.L., Catherine, A., Bellucci, A., Bao, Q., Chang, P., Corti, S., Fučkar, N.S., Guemas, V., Von Hardenberg, J., Hazeleger, W., Kodama, C., Koenigk, T., Leung, L.R., Lu, J., Luo, J.J., Mao, J., Mizielinski, M.S., Mizuta, R., Nobre, P., Satoh, M., Scoccimarro, E., Semmler, T., Small, J., Von Storch, J.S., 2016. High resolution model Intercomparison project (HighResMIP v1.0) for CMIP6. Geosci. Model Dev. (GMD). https://doi.org/10.5194/gmd-9-4185-2016.

Hamed, K.H., Rao, A.R., 1998. A modified Mann-Kendall trend test for autocorrelated data. J. Hydrol. 204, 182–196. https://doi.org/10.1016/S0022-1694(97)00125-X.

Hasselmann, K., 1993. Optimal fingerprints for the detection of time-dependent climate change. J. Clim. 2. https://doi.org/10.1175/1520-0442(1993)006<1957:OFFTDO>2.0.CO.

Hayhoe, K., Wuebbles, D.J., Easterling, D.R., Fahey, D.W., Doherty, S., Kossin, J., Sweet, W., Vose, R., Wehner, M., 2018. Our changing climate. In impacts, risks, and adaptation in the United States: fourth national climate assessment, volume II. In: Impacts, Risks, and Adaptation in the United States: Fourth National Climate Assessment, ume II. https://doi.org/10.7930/NCA4.2018.CH2.

Hegerl, G., Zwiers, F., 2011. Use of models in detection and attribution of climate change. Wiley Interdiscip. Rev. Clim. Chang. https://doi.org/10.1002/wcc.121.

Hoerling, M., Eischeid, J., Perlwitz, J., Quan, X.-W., Wolter, K., Cheng, L., Hoerling, M., Eischeid, J., Perlwitz, J., Quan, X.-W., Wolter, K., Cheng, L., 2016. Characterizing recent trends in U.S. Heavy precipitation. J. Clim. 29, 2313–2332. https://doi.org/10.1175/JCLI-D-15-0441.1.

Huang, B., Thorne, P.W., Banzon, V.F., Boyer, T., Chepurin, G., Lawrimore, J.H., Menne, M.J., Smith, T.M., Vose, R.S., Zhang, H.M., 2017a. Extended reconstructed Sea surface temperature, Version 5 (ERSSTv5): upgrades, validations, and intercomparisons. J. Clim. https://doi.org/10.1175/JCLI-D-16-0836.1.

Huang, H., Winter, J.M., Osterberg, E.C., 2018. Mechanisms of abrupt extreme precipitation change over the northeastern United States. J. Geophys. Res. Atmos. https://doi.org/10.1029/2017JD028136.

Huang, H., Winter, J.M., Osterberg, E.C., Horton, R.M., Beckage, B., 2017b. Total and extreme precipitation changes over the Northeastern United States. J. Hydrometeorol. https://doi.org/10.1175/JHM-D-16-0195.1. JHM-D-16-0195.1.

Ivancic, T.J., Shaw, S.B., 2016. A U.S.-based analysis of the ability of the Clausius-Clapeyron relationship to explain changes in extreme rainfall with changing temperature. J. Geophys. Res. https://doi.org/10.1002/2015JD024288.

Kay, J.E., Deser, C., Phillips, A., Mai, A., Hannay, C., Strand, G., Arblaster, J.M., Bates, S. C., Danabasoglu, G., Edwards, J., Holland, M., Kushner, P., Lamarque, J.-F., Lawrence, D., Lindsay, K., Middleton, A., Munoz, E., Neale, R., Oleson, K., Polvani, L., Vertenstein, M., Kay, J.E., Deser, C., Phillips, A., Mai, A., Hannay, C., Strand, G., Arblaster, J.M., Bates, S.C., Danabasoglu, G., Edwards, J., Holland, M., Kushner, P., Lamarque, J.-F., Lawrence, D., Lindsay, K., Middleton, A., Munoz, E., Neale, R., Oleson, K., Polvani, L., Vertenstein, M., 2015. The community earth system model (CESM) large ensemble project: a community resource for studying climate change in the presence of internal climate variability. Bull. Am. Meteorol. Soc. 96, 1333–1349. https://doi.org/10.1175/BAMS-D-13-00255.1.

Kerr, R.A., 2000. A north atlantic climate pacemaker for the centuries. Science 288. https://doi.org/10.1126/science.288.5473.1984, 1984–5.

Kim, W.M., Yeager, S., Chang, P., Danabasoglu, G., 2018a. Low-frequency North Atlantic climate variability in the community earth system model large ensemble. J. Clim. https://doi.org/10.1175/JCLI-D-17-0193.1.

Kim, W.M., Yeager, S.G., Danabasoglu, G., 2018b. Key role of internal ocean dynamics in atlantic multidecadal variability during the last half century. Geophys. Res. Lett. https://doi.org/10.1029/2018GL080474.

Kirchmeier-Young, M.C., Zhang, X., 2020. Human influence has intensified extreme precipitation in North America. Proc. Natl. Acad. Sci. Unit. States Am. https://doi.org/10.1073/pnas.1921628117, 201921628.

Kunkel, K.E., Easterling, D.R., Kristovich, D.A.R., Gleason, B., Stoecker, L., Smith, R., 2010. Recent increases in U.S. heavy precipitation associated with tropical cyclones. Geophys. Res. Lett. 37, 2–5. https://doi.org/10.1029/2010GL045164.

Kunkel, K.E., Easterling, D.R., Kristovich, D.A.R., Gleason, B., Stoecker, L., Smith, R., Kunkel, K.E., Easterling, D.R., Kristovich, D.A.R., Gleason, B., Stoecker, L., Smith, R., 2012. Meteorological causes of the secular variations in observed extreme precipitation events for the conterminous United States. J. Hydrometeorol. 13, 1131–1141. https://doi.org/10.1175/JHM-D-11-0108.1.

Kunkel, K.E., Karl, T.R., Brooks, H., Kossin, J., Lawrimore, J.H., Arndt, D., Bosart, L., Changnon, D., Cutter, S.L., Doesken, N., Emanuel, K., Groisman, P.Y., Katz, R.W., Knutson, T., O'brien, J., Paciorek, C.J., Peterson, T.C., Redmond, K., Robinson, D., Trapp, J., Vose, R., Weaver, S., Wehner, M., Wolter, K., Wuebbles, D., 2013. Monitoring and understanding trends in extreme storms: state of knowledge. Bull. Am. Meteorol. Soc. 94, 499–514. https://doi.org/10.1175/BAMS-D-11-00262.1.

Mankin, J.S., Lehner, F., Coats, S., McKinnon, K.A., 2020. The value of initial condition large ensembles to robust adaptation decision-making. Earth's Futur. https://doi.org/10.1029/2020ef001610.

Mann, M.E., Rahmstorf, S., Kornhuber, K., Steinman, B.A., Miller, S.K., Coumou, D., 2017. Influence of anthropogenic climate change on planetary wave resonance and extreme weather events. Nat. Publ. Gr. https://doi.org/10.1038/srep45242.

Mann, M.E., Steinman, B.A., Brouillette, D.J., Miller, S.K., 2021. Multidecadal climate oscillations during the past millennium driven by volcanic forcing. Science 80, 1014–1019. https://doi.org/10.1126/science.abc5810, 371.

Mann, M.E., Steinman, B.A., Miller, S.K., 2020. Absence of internal multidecadal and interdecadal oscillations in climate model simulations. Nat. Commun. https://doi.org/10.1038/s41467-019-13823-w.

Mann, M.E., Steinman, B.A., Miller, S.K., 2014. On forced temperature changes, internal variability, and the AMO. Geophys. Res. Lett. https://doi.org/10.1002/2014GL059233.

Marquardt Collow, A.B., Bosilovich, M.G., Koster, R.D., Collow, A.B.M., Bosilovich, M.G., Koster, R.D., 2016. Large-scale influences on summertime extreme precipitation in the northeastern United States. J. Hydrometeorol. 17, 3045–3061. https://doi.org/10.1175/JHM-D-16-0091.1.

Martel, J.-L., Mailhot, A., Brissette, F., Caya, D., 2018. Role of natural climate variability in the detection of anthropogenic climate change signal for mean and extreme precipitation at local and regional scales. J. Clim. 31, 4241–4263. https://doi.org/10.1175/JCLI-D-17-0282.1.

Menne, M.J., Durre, I., Vose, R.S., Gleason, B.E., Houston, T.G., Menne, M.J., Durre, I., Vose, R.S., Gleason, B.E., Houston, T.G., 2012. An overview of the global historical Climatology network-daily database. J. Atmos. Ocean. Technol. 29, 897–910. https://doi.org/10.1175/JTECH-D-11-00103.1.

Min, S.K., Zhang, X., Zwiers, F.W., Hegerl, G.C., 2011. Human contribution to more-intense precipitation extremes. Nature. https://doi.org/10.1038/nature09763.

Minter, S., 2012. Irene Recovery – Overview. Agency of Administration, State of Vermont. https://ljfo.vermont.gov/assets/docs/reports/Legislative-Briefings/36e65b9238/2012_11_28_Minter_Irene_Recovery.pdf.

Mitchell, J.F.B., Karoly, D.J., 2001. Detection of climate change and attribution of causes. Third IPCC assess. Report. Work. Gr. I Sci. Basis.

Murakami, H., Delworth, T.L., Cooke, W.F., Zhao, M., Xiang, B., Hsu, P.-C., 2020. Detected climatic change in global distribution of tropical cyclones. Proc. Natl. Acad. Sci. Unit. States Am. 117, 10706–10714. https://doi.org/10.1073/pnas.1922500117.

Murakami, H., Levin, E., Delworth, T.L., Gudgel, R., Hsu, P.C., 2018. Dominant effect of relative tropical Atlantic warming on major hurricane occurrence. Science 80. https://doi.org/10.1126/science.aat6711.

Murphy, L.N., Bellomo, K., Cane, M., Clement, A., 2017. The role of historical forcings in simulating the observed Atlantic multidecadal oscillation. Geophys. Res. Lett. 44, 2472–2480. https://doi.org/10.1002/2016GL071337.

Myhre, G., Shindell, D., Bréon, F.-M., Collins, W., Fuglestvedt, J., Huang, J., Koch, D., Lamarque, J.-F., Lee, D., Mendoza, B., Nakajima, T., Robock, A., Stephens, G., Takemura, T., Zhang, H., 2013. Anthropogenic and natural radiative forcing. Climate Change 2013 the Physical Science Basis: Working Group I Contribution to the Fifth Assessment Report of the Intergovernmental Panel on Climate Change. https://doi.org/10.1017/CBO9781107415324.018.

Ntelekos, A.A., Smith, J.A., Donner, L., Fast, J.D., Gustafson, W.I., Chapman, E.G., Krajewski, W.F., 2009. The effects of aerosols on intense convective precipitation in the northeastern United States. Q. J. R. Meteorol. Soc. https://doi.org/10.1002/qj.476.

Otterå, O.H., Bentsen, M., Drange, H., Suo, L., 2010. External forcing as a metronome for Atlantic multidecadal variability. Nat. Geosci. 3, 688–694. https://doi.org/10.1038/ngeo955.

Peterson, T.C., Heim, R.R., Hirsch, R., Kaiser, D.P., Brooks, H., Diffenbaugh, N.S., Dole, R.M., Giovannettone, J.P., Guirguis, K., Karl, T.R., Katz, R.W., Kunkel, K., Lettenmaier, D., McCabe, G.J., Paciorek, C.J., Ryberg, K.R., Schubert, S., Silva, V.B. S., Stewart, B.C., Vecchia, A.V., Villarini, G., Vose, R.S., Walsh, J., Wehner, M., Wolock, D., Wolter, K., Woodhouse, C.A., Wuebbles, D., Peterson, T.C., Jr, R.R.H., Hirsch, R., Kaiser, D.P., Brooks, H., Diffenbaugh, N.S., Dole, R.M., Giovannettone, J. P., Guirguis, K., Karl, T.R., Katz, R.W., Kunkel, K., Lettenmaier, D., McCabe, G.J., Paciorek, C.J., Ryberg, K.R., Schubert, S., Silva, V.B.S., Stewart, B.C., Vecchia, A.V., Villarini, G., Vose, R.S., Walsh, J., Wehner, M., Wolock, D., Wolter, K., Woodhouse, C.A., Wuebbles, D., 2013. Monitoring and understanding changes in heat waves, cold waves, floods, and droughts in the United States: state of knowledge. Bull. Am. Meteorol. Soc. 94, 821–834. https://doi.org/10.1175/BAMS-D-12-00066.1.

Qin, M., Dai, A., Hua, W., 2020. Aerosol-forced multidecadal variations across all ocean basins in models and observations since 1920. Sci. Adv. https://doi.org/10.1126/sciadv.abb0425.

Ribes, A., Planton, S., Terray, L., 2013. Application of regularised optimal fingerprinting to attribution. Part I: method, properties and idealised analysis. Clim. Dynam. https://doi.org/10.1007/s00382-013-1735-7.

Roberts, M.J., Camp, J., Seddon, J., Vidale, P.L., Hodges, K., Vanniere, B., Mecking, J., Haarsma, R., Bellucci, A., Scoccimarro, E., Caron, L.P., Chauvin, F., Terray, L., Valcke, S., Moine, M.P., Putrasahan, D., Roberts, C., Senan, R., Zarzycki, C., Ullrich, P., 2020. Impact of model resolution on tropical cyclone simulation using the HighResMIP-PRIMAVERA multimodel ensemble. J. Clim. https://doi.org/10.1175/JCLI-D-19-0639.1.

Saba, V.S., Griffies, S.M., Anderson, W.G., Winton, M., Alexander, M.A., Delworth, T.L., Hare, J.A., Harrison, M.J., Rosati, A., Vecchi, G.A., Zhang, R., 2016. Enhanced warming of the northwest atlantic ocean under climate change. J. Geophys. Res. Ocean. https://doi.org/10.1002/2015JC011346.

Santer, B.D., Fyfe, J.C., Solomon, S., Painter, J.F., Bonfils, C., Pallotta, G., Zelinka, M.D., 2019. Quantifying stochastic uncertainty in detection time of human-caused climate signals. Proc. Natl. Acad. Sci. U. S. A. https://doi.org/10.1073/pnas.1904586116.

Sarojini, B.B., Stott, P.A., Black, E., 2016. Detection and attribution of human influence on regional precipitation. Nat. Clim. Change. https://doi.org/10.1038/nclimate2976.

Si, D., Hu, A., Si, D., Hu, A., 2017. Internally generated and externally forced multidecadal oceanic modes and their influence on the summer rainfall over east asia. J. Clim. 30, 8299–8316. https://doi.org/10.1175/JCLI-D-17-0065.1.

Sobel, A.H., Camargo, S.J., Hall, T.M., Lee, C.Y., Tippett, M.K., Wing, A.A., 2016. Human influence on tropical cyclone intensity. Science 80. https://doi.org/10.1126/science.aaf6574.

Stone, D.A., Allen, M.R., Stott, P.A., Pall, P., Min, S.-K., Nozawa, T., Yukimoto, S., 2009. The detection and attribution of human influence on climate. Annu. Rev. Environ. Resour. https://doi.org/10.1146/annurev.environ.040308.101032.

Ting, M., Camargo, S.J., Li, C., Kushnir, Y., 2015. Natural and forced North Atlantic hurricane potential intensity change in CMIP5 models. J. Clim. https://doi.org/10.1175/jcli-d-14-00520.1.

Ting, M., Kushnir, Y., Li, C., 2014. North Atlantic multidecadal SST oscillation: external forcing versus internal variability. J. Mar. Syst. https://doi.org/10.1016/j.jmarsys.2013.07.006.

van der Wiel, K., Kapnick, S.B., Vecchi, G.A., Cooke, W.F., Delworth, T.L., Jia, L., Murakami, H., Underwood, S., Zeng, F., 2016. The resolution dependence of contiguous U.S. precipitation extremes in response to CO2 forcing. J. Clim. https://doi.org/10.1175/JCLI-D-16-0307.1.

Villarini, G., Vecchi, G.A., 2013. Projected increases in North Atlantic tropical cyclone intensity from CMIP5 models. J. Clim. https://doi.org/10.1175/JCLI-D-12-00441.1.

Wan, H., Zhang, X., Zwiers, F., Min, S.K., 2015. Precipitation change over the period 1966–2005 to huAttributing northern high-latitude man influence. Clim. Dynam. https://doi.org/10.1007/s00382-014-2423-y.

Winter, J.M., Huang, H., Osterberg, E.C., Mankin, J.S., 2020. Anthropogenic impacts on the exceptional precipitation of 2018 in the mid-Atlantic United States. Bull. Am. Meteorol. Soc. https://doi.org/10.1175/BAMS-D-19-0172.1.

Zhang, R., 2008. Coherent surface-subsurface fingerprint of the Atlantic meridional overturning circulation. Geophys. Res. Lett. https://doi.org/10.1029/2008GL035463.

Zhang, R., Sutton, R., Danabasoglu, G., Kwon, Y.O., Marsh, R., Yeager, S.G., Amrhein, D. E., Little, C.M., 2019. A review of the role of the atlantic meridional overturning circulation in atlantic multidecadal variability and associated climate impacts. Rev. Geophys. https://doi.org/10.1029/2019RG000644.

Zhang, X., Wan, H., Zwiers, F.W., Hegerl, G.C., Min, S.K., 2013. Attributing intensification of precipitation extremes to human influence. Geophys. Res. Lett. https://doi.org/10.1002/grl.51010.